Materials Research. 2023; 26:e20220195
DOI: https://doi.org/10.1590/1980-5373-MR-2022-0195

A New Two-Step Method for Laser Cladding of Silicon Carbide in Wc-Co Substrates

***Renê Martins Volu*[a,b]*, *Kahl Zilnyk*[a], *Silvelene Alessandra Silva Dyer*[b], *Claudio Luis dos Santos*[b,c], *Jonas Jakutis Neto*[a,b], *Getúlio de Vasconcelos*[b]**

[a]*Instituto Tecnológico de Aeronáutica (ITA), São Jose dos Campos, SP, Brasil.*
[b]*Instituto de Estudos Avançados (IEAv), São Jose dos Campos, SP, Brasil.*
[c]*Instituto Federal de São Paulo (IFSP), São José dos Campos, SP, Brasil.*

Received: April 13, 2022; Revised: October 29, 2022; Accepted: December 11, 2022

WC-Co cutting tools are widely used by the metalworking industry. In order to improve the properties of these tools, research on the application of wear-resistant coatings, such as polycrystalline diamond, are of great importance to several applications. It is known that the occurrence of high-stress levels between the coating and the substrate can lead to adhesion failures. One strategy to minimize these failures is applying an intermediate layer of SiC. In this work, the deposition of a SiC layer was carried out by a novel two-step laser cladding approach. Instead of cladding directly the pre-synthesized SiC on the substrates, a 200 µm silicon powder layer was pre-deposited on the WC-Co substrates and then irradiated with a 30 W CO_2 laser. To improve metallurgical bonding between the tungsten and the Si layer, all substrates were chemically attacked. This attack allows cobalt removal from the surface and increases surface roughness, improving the laser cladding process. After the SiC laser cladding, samples were coated with a 200 µm graphite powder layer and irradiated again by a CO_2 laser. The samples were characterized by SEM, EDS, and XRD analysis. The results showed that in the first step, an irradiation energy of about 0.27 J was enough to fuse the silicon powder to the substrate and in the second step, 0.13 J was enough to promote the reaction between silicon, carbon and the WC substrate, resulting in the *in-situ* synthesis of SiC. Finally, a new method was proposed for the deposition of SiC on WC-Co based substrates and the observed results allowed the proposal of an empirical equation to describe the chemical reactions of the process.

Keywords: *Laser cladding, cutting tools, tungsten carbide, silicon carbide.*

1. Introduction

Since their conception in 1923, carbide tools (WC-Co) are the most widely used cutting tools in the metalworking industry. However, given the constant development of new alloys and the pursuit of increased productivity, the use of hard coatings has become a standard to increase the wear resistance of tools set for high speed cutting and feed[1,2]. As an example, diamond coatings are considered a great option for the task, due to their chemical, physical and mechanical properties, in addition to its extremely high hardness (10000 HV)[3,4].

Adding a diamond coating to the WC-Co substrate results in tools with extremely hard surfaces and tough cores increasing the tool lifetime during the machining process. Nevertheless, diamond-coated WC-Co tooling presents some technological challenges to be overcome, such as: incompatibility between the thermal expansion coefficients of the diamond film ($1x10^{-6}$ / ° C) and the WC-Co substrate ($5.5\text{-}7x10^{-6}$ / ° C); presence of Co on the tool surface which may promote the formation of graphite. Both drawbacks favor coating peeling[5-7]. In order to avoid that, chemical etching is usually used to reduce cobalt concentration on the surface and to increase the interface roughness, improving the metallurgical bond between the substrate and the deposited film[8]. Laser irradiation has also been reported as an effective method to remove Co from the outermost layer of WC-Co[9]. Another viable strategy is the deposition of intermediate layers, acting as diffusion barriers for Co and minimizing effects from the thermal expansion difference. Among several possible interlayers cited in the literature, silicon carbide (SiC) is pointed as one of the best options for such application[7,10-20]. SiC is extensively used in abrasive tools, ceramics, insulation, metallurgical applications, refractories, and wear resistant materials, and this is due to its superior properties, including wide bandgap, low density, low thermal expansion, excellent thermal shock/oxidation/chemical resistance, high hardness, and high thermal conductivity[18,21].

Traditionally, SiC interlayers are grown by Hot Filament Chemical Vapor Deposition (HFCVD), however, Contin et al.[6] have shown the viability of producing interlayers irradiating a laser beam on a SiC powder layer dispersed over the substrate surface. According to the authors[6], the advantages of laser deposition are higher processing speed, higher heating/cooling rate, better precision, possibility of automation and versatility.

The main mechanism of the process cited in[6] is the sintering of SiC. This work proposes a new methodology

*e-mail: rmvolu@gmail.com

to create a SiC interlayer tightly bonded to the WC-Co substrate which is not sintering. The procedure consists of fusing a silicon layer on the substrate using a laser then covering it with carbon and irradiating it again with the laser to synthesize SiC *in-situ*. Silicon melting temperature (1414 °C) is considerably lower than the temperatures required to promote the sintering of SiC particles (about 1950 ~ 2180 °C[22,23]), making it possible to use low power, inexpensive CO_2 lasers in the process. Furthermore, the complete melting of the silicon layer could promote a tighter substrate bonding than the solid-state sintering of SiC particles. It was previously verified by Tóth et al.[24] that using ultrafast lasers (fs), this reaction can be obtained, and according to Galvão et al.[25], the carbonation of a solid SiC target using a CO_2 laser is also possible.

2. Materials and Methods

2.1. WC-Co substrate preparation

The SANDVIK Brand R262.22-1304 commercial machining tools (inserts), shown in Figure 1, were used as samples in this work. To remove the cobalt and consequently increase the surface energy, the WC-Co samples were subjected to two chemical treatments. First, the samples were immersed in Murakami's reagent ($K_3(Fe(CN)_6)$ + KOH + H_2O) for 10 minutes in order to dissolve the WC particles from the surface, exposing the Co layer. In the second step, the samples were immersed in aqua regia (HNO_3 / HCl = 1: 3) for 5 minutes to remove the Co from the outermost layer.

2.2. Silicon pre-deposition

A mixture of silicon powder (50 g) and ethylic alcohol (300 ml) was sprayed through a pneumatic gun, as shown in Figure 2. The air pressure used in the gun was adjusted to ensure good transport of the mixture to the substrate (~ 3 Bar). After spraying, the samples were dried at 60° C for residual alcohol evaporation. The thickness of the pre-deposited powder layer was controlled using the scratching technique. It consists of scratching the pre-deposited powder layer with a tip of known geometry (in this case, a 60° edge), positioned perpendicularly to the sample surface and pressed by a polymeric spring (biaxially-oriented polyethylene terephthalate "Mylar®, Dupont Tejjin Films"). The table is horizontally moved, resulting in a scratch on the powder layer. Measuring the width of the scratch under an optical microscope and using trigonometric relationships, the thickness of the pre-deposited layer is calculated. In this work, a powder layer thickness of 200 ± 20 µm was used for all tests[26,27]. Figure 3 illustrates the scratching process of the pre-deposited powder layer.

2.3. Laser cladding process

The laser fusion process used in this work is referred to as "laser cladding" in the literature. During cladding, the laser beam is absorbed by the sample layer causing fast heating (10^6 K / s), and when the laser stops it cools down dissipating heat in the substrate[28,29].

In order to melt or vaporize the powder, it is necessary to provide a certain amount of energy. The interaction time, *t*, of a laser beam on a surface, is an important variable to determine the amount of absorbed energy. In a CO_2 laser, which operates in continuous mode, the interaction time can be estimated by the ratio between laser spot size, *2ω (diameter)*, and laser beam scanning speed, *v*, over the sample, described by Equation 1[29]:

$$t = 2\omega / v \quad (1)$$

Given the power, *P*, and the interaction time of the laser beam, it is possible to determine the amount of heat and/or energy, *Q*, delivered to the system, described by Equation 2[29]:

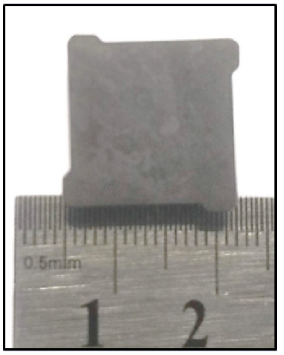

Figure 1. WC-Co cutting tool used as substrate in this work.

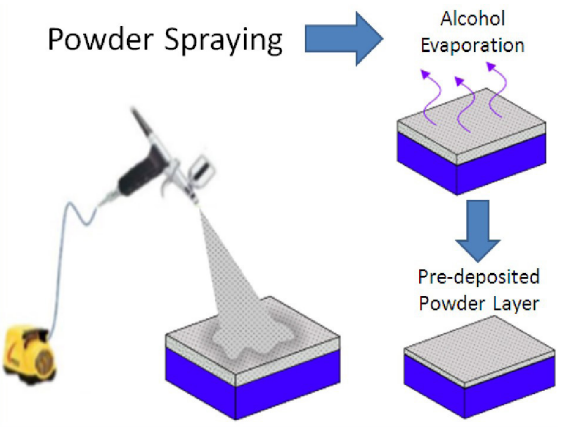

Figure 2. Procedure to create the pre-deposited silicon layer.

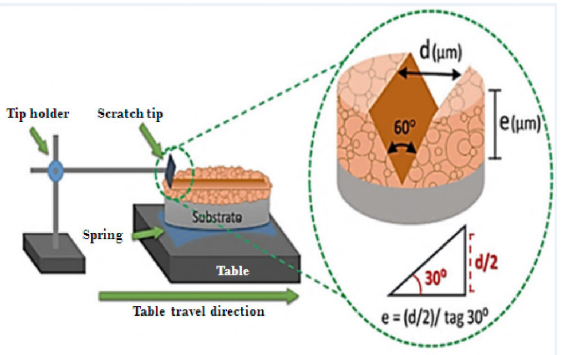

Figure 3. Schematic drawing of the scratching technique to evaluate the thickness of the pre-deposited powder layer.

$$Q = P \bullet t \quad (2)$$

The silicon layer was deposited by laser cladding using a Synrad CO_2 Laser emitting at 10.6 µm in continuous wave mode with a maximum power of 30 W. Beam delivery system was composed of a scanner with a focusing theta lens (focal length of 125 ± 2 mm), and the following scan parameters: scanning speed of 20 mm/s, 50% overlap between laser tracks and beam diameter of 180 µm. According to Equation 2, at this condition the laser irradiation energy was of 0.27 J. During the laser irradiation process, a nitrogen gas flow (5 L/min) was used to protect the optics as well as to minimize undesirable reactions of the irradiated sample with atmospheric contents.

2.4. Graphite pre-deposition and laser cladding

A mixture of graphite powder (30 g) and ethylic alcohol (300 ml) was sprayed onto the previously cladded silicon layer samples using a pneumatic gun. A 200 ± 20 µm layer of graphite was sprayed (as defined by the scratching process) over chemically treated and cladded samples followed by CO_2 laser irradiation performed with a laser scanning speed of 40 mm/s, delivering a laser irradiation energy of 0.13 J.

2.5. Chemical and microstructural characterization

Scanning electron microscopy (SEM) images from the samples were obtained with a TESCAN MIRA3 field-emission gun (FEG) microscope and a Tescan VEGA3 tungsten filament microscope, both operated in the secondary electron detection mode. Energy dispersive spectroscopy (EDS) was used (in both microscopes) to analyze the chemical composition of the samples.

The observed phases were identified using a Panalytical Empyrean X-ray diffractometer (XRD), with a Cu-Kα radiation source, and then quantified using the HighScore Plus software supported by the Inorganic Crystal Structure Database (ICSD) and using Rietveld refinement. Substrate roughness was measured, before and after the chemical treatments, using a TAYLOR HOBSON/TALYSURF profilometer.

3. Results and Discussion

3.1. Substrate preparation

The surface morphology of the substrate is shown in Figure 4 where it is possible to observe the shape of the WC grains. WC-Co substrate chemical composition, as-received, was obtained by EDS and is presented in Table 1. It is important to emphasize that the Co element is responsible for the liquid phase formation and Ti, Ta, and Al are additional elements used to improve material properties[30]. The light-weighted elements, like C and O, were detected but not considered for the EDS quantification.

The WC-Co substrate was submitted to XRD analysis to evaluate the phases present on the surface and the diffractogram obtained is shown in Figure 5(a). Only peaks belonging to the WC (ICSD 98-000-3871 – Space Group P -6 m 2) phase are visible. An evaluation of the substrate roughness was carried out in three distinct regions of the samples, presenting average roughness (Ra) of 0.211 µm, with a standard deviation of 0.015 µm.

Murakami's reagent was used to dissolve the surface WC from the samples which is required for the Co removal in the next step. The SEM micrograph of the etched sample is shown in Figure 6 where it is possible to verify the dissolution of WC grains. Dissolution of the WC grains was confirmed by EDS shown in Table 1, where a decreasing in W content and an increasing in Co content near the surface is observed. Another consequence of the etching is the increase in average surface roughness (Ra) to 0.299 µm, with a standard deviation of 0.020 µm.

In the second chemical treatment, aqua regia was used for the Co removal from the sample surface. The average surface roughness (Ra) was reduced to 0.269 µm, with a

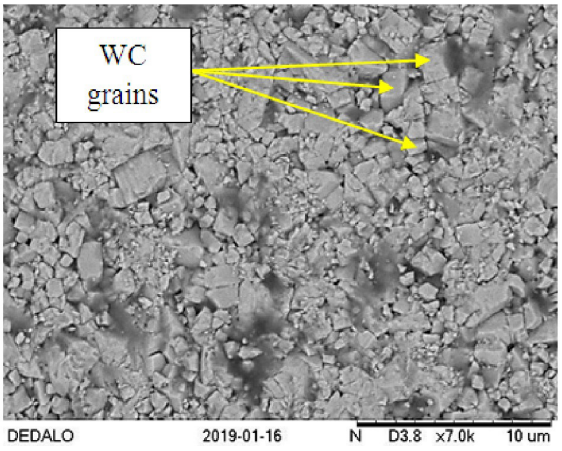

Figure 4. SEM image of WC-Co substrate surface, as received.

Table 1. Chemical composition of WC-Co substrate and cladded layers, measured by EDS.

	Al		Ti		Co		Ta		W		Si	
	%wt	±SD	%wt	±SD	%wt	±SD	%wt	±SD	%wt	±SD	%wt	±SD
As-received WC-Co	**7.61**	0.59	**19.84**	6.06	**20.73**	1.60	**7.94**	1.86	**43.88**	2.70	--	--
After Murakami's	**6.75**	0.65	**55.42**	10.43	**26.87**	2.35	**4.61**	1.62	**6.32**	1.65	--	--
After aqua regia	--	--	**16.46**	4.36	**3.71**	0.72	**16.03**	1.62	**63.79**	2.94	--	--
After Si cladding (no chemical etching)	--	--	--	--	**0.47**	0.23	--	--	**37.98**	0.61	**61.56**	0.40
After chemical etching and Si cladding	--	--	--	--	**0.28**	0.38	--	--	**40.96**	0.95	**58.77**	0.64
After graphite depostion	--	--	--	--	--	--	--	--	**2.52**	0.25	**97.48**	0.25

standard deviation of 0.025 μm, when compared to those obtained in the previous step. SEM image (Figure 7) shows the surface of the sample etched by aqua regia. The reduction of Co content on the surface of the WC-Co sample is visible and it was confirmed by an EDS analysis (Table 1).

3.2. Laser cladding of the silicon layer

Aiming to test the efficiency of the chemical attack, laser cladding of the Si layer was performed in two groups of samples, one with chemical treatment and the other without. The clad samples were analyzed by SEM and EDS, and the results of these analysis are also presented in Table 1. Figure 8 shows a discontinuous coating consisting of fused, sintered, and coalesced silicon grains. Figure 9 brings the chemically treated sample SEM where it is possible to verify the silicon grains evenly distributed on the sample surface. For the two samples, the EDS results confirm cobalt depletion and the presence of silicon on the surfaces.

XRD was performed after Si cladding in both samples, with and without chemical treatment. From the diffraction

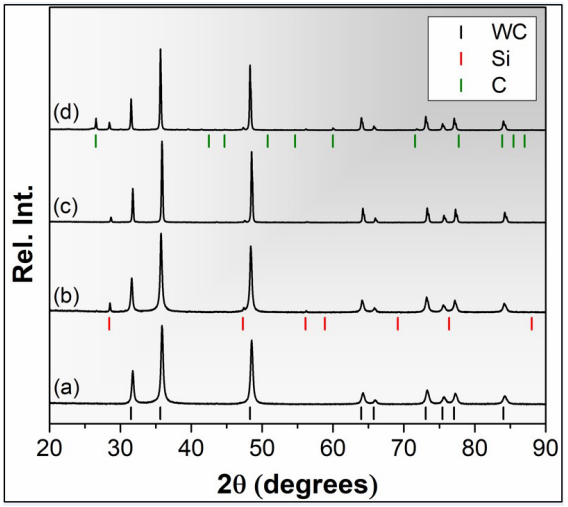

Figure 5. XRD of samples: a) as-received WC-Co sample; b) sample without chemical treatment, after laser cladding of the Si layer, c) sample with chemical treatment, after laser cladding of the Si layer; and d) sample after Si and graphite cladding.

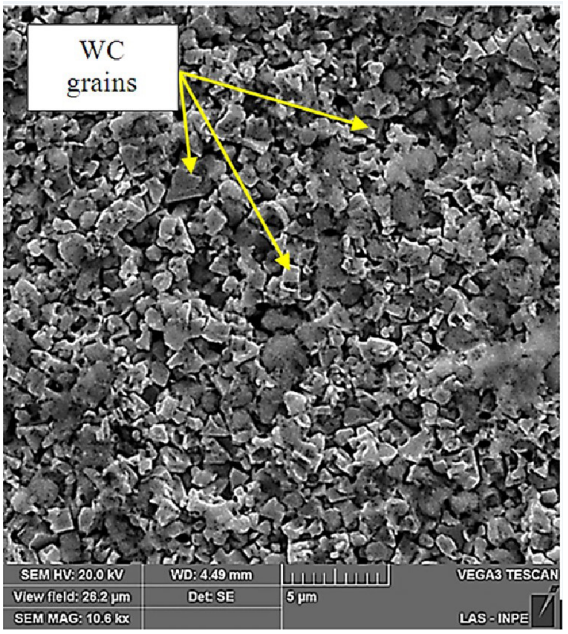

Figure 7. SEM micrograph of the WC-Co sample etched for 5 min with aqua regia.

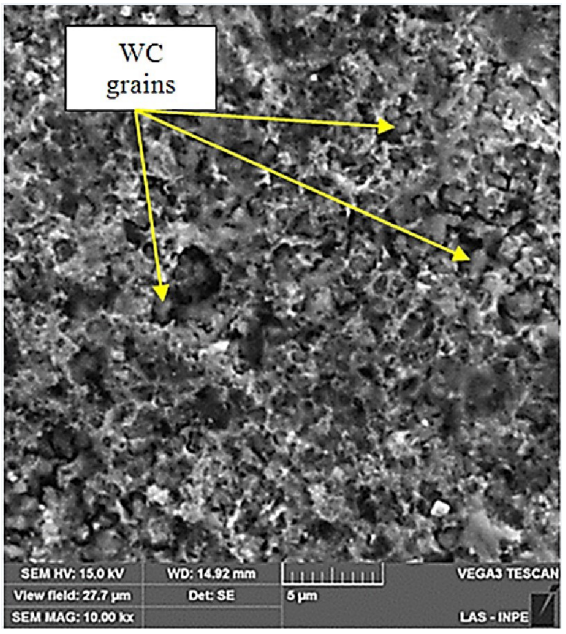

Figure 6. SEM image of WC-Co substrate, after 10 min immersion in Murakami's reagent.

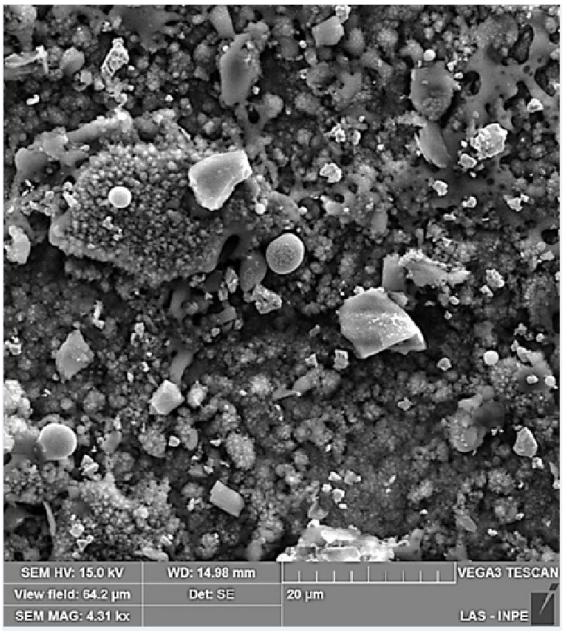

Figure 8. WC-Co sample without chemical etching, after CO_2 laser irradiation.

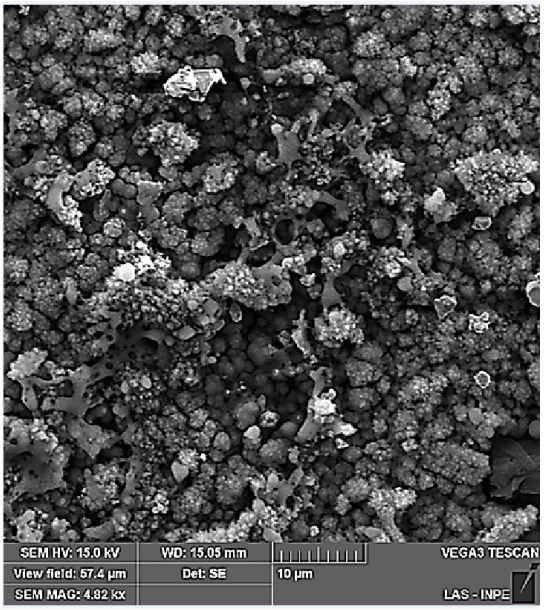

Figure 9. WC-Co sample with chemical etching, after CO_2 laser irradiation.

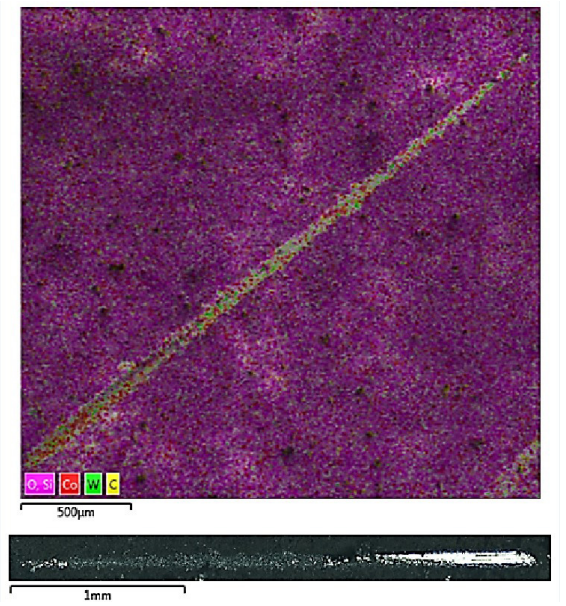

Figure 10. EDS mapping of scratch test on the sample without acid treatment.

profiles shown in Figures 5(b) and (c), it can be seen that WC peaks, already observed in the as-received sample, are still present and they belong to silicon (ICSD 98-004-8899 – space Group F d -3 m). The absence of other peaks strongly suggests that there were no reactions between the cladded Si and the WC substrate. Also, according to the diffractograms, there was no substantial difference between the samples with or without chemical treatment.

Scratch tests were performed on the chemically treated and untreated samples by applying a progressive load from 3 to 30 N on a 3 mm test track. Elements present in the region of the scratch test were identified by EDS and the morphology of the scratch was analyzed by optical microscopy.

In the sample without chemical treatment, the presence of silicon in the scratched region was not identified. This fact is an indicative that there was a weaker adhesion of the coating to the substrate. On the other hand, the sample with chemical treatment presented silicon up to approximately 1.5 mm of the scratch, suggesting that the coating resisted a load of 15 mN. These results are presented in Figures 10 and 11, proving the efficiency of the acid treatment in relation to silicon coating adhesion. This ability to withstand the scratch test can be attributed to the increased surface energy of the sample after chemical treatment.

3.3. Graphite irradiation

The irradiated samples were analyzed by SEM, EDS, and XRD. Table 1 presents the EDS results indicating only the presence of silicon (carbon was also detected but not considered for all performed EDS analyses). SEM micrographs (Figure 12) revealed sintered structures suggesting SiC formation.

In a first analysis of the XRD shown in Figure 5(d), the presence of peaks referring to the WC, Si, and 2H-graphite (ICSD 98-006-1028 - Space Group P 63 m c) phases is clearly visible. However, low intensity peaks not belonging to these phases can be observed close to the background. These peaks were indexed as belonging to the following phases: silicon carbide (SiC) (ICSD 98-001-1882 - Space Group F -4 3 m), tungsten silicide (WSi2) (ICSD 98-003-1268 - Space Group I 4 / mmm) and ditungsten carbide (W_2C) (ICSD 98-006-2179 - P 63 / mmc). The presence of these phases is a strong indication that there was some dissociation of the WC present in the substrate and subsequent reaction with the cladded Si and C. Although the laser energy applied in this stage (0.13 J) is lower than in the Si coating (0.27 J), it was enough to generate WSi_2 and SiC phases. The decomposition of WC to form WSi_2 and W_2C is thermodynamically expected[31,32], as expressed in equations 3 and 4[27,28], but it did not occur during Si layer irradiation. It may be related to the lack of energy required for such transformation, which only occurred after the deposition of graphite which presents higher absorptivity at the wavelength of the CO_2 laser (absorptivities of: Si α = 1.4499 cm^{-1} / C α = 44608 cm^{-1})[33,34], thus increasing the temperature on the sample surface and favoring the reaction between W and Si. According to Nanda Kumar et al.[32], this reaction occurs at temperatures above 1200 ° C, but it was not observed after the first irradiation or it was quite limited and the products were not detected by XRD, probably due to the lack of kinetic conditions (short irradiation time). This reaction is markedly exothermic (DeltaH = -41 kJ/mol) and leads to a significant adiabatic "chemical heating". Temperature during the sintering of a WC-Si system can reach nearly 1800 °C due to the occurrence of such reaction. On the other hand, the formation of SiC is not expected in this equation, but may have occurred through Si reaction with the deposited C.

$$WC + 2Si = WSi_2 + C_{(graphite/a-Carbon)} \quad (3)$$

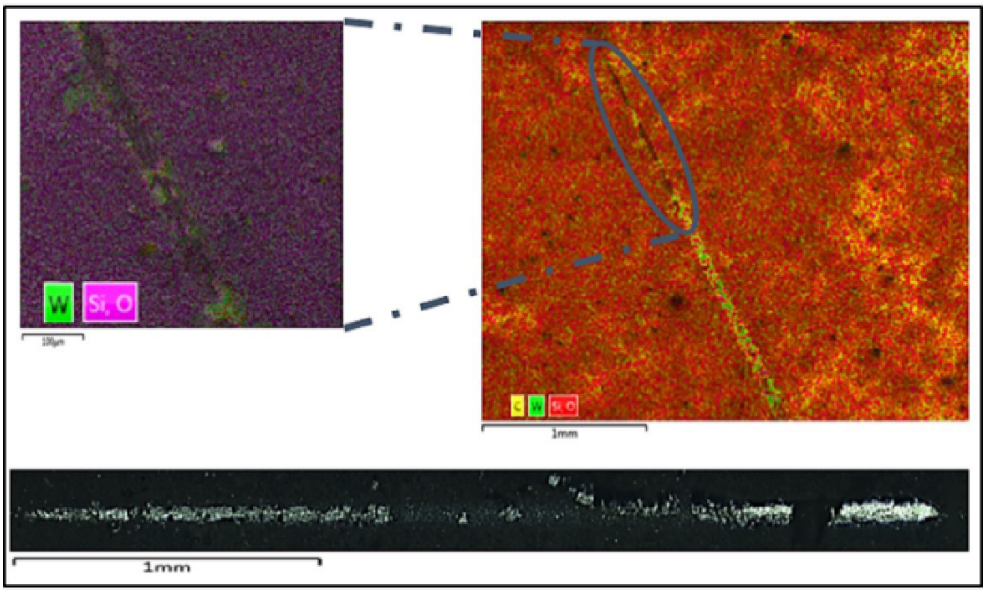

Figure 11. EDS mapping of scratch test on the sample with acid treatment.

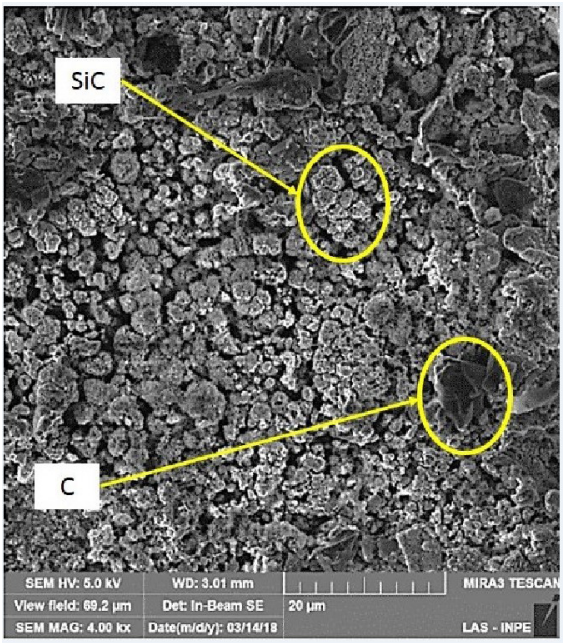

Figure 12. SEM micrograph of the WC-Co sample after Si cladding, graphite coating, and CO_2 laser irradiation.

$$2WC + O_2 = W_2C + CO_2 \quad (4)$$

The volume fraction of the phases formed in the sample, after graphite cladding, was estimated using Rietveld refinement and the result is shown in Figure 13. For better visualization, the low-intensity peaks, indexed as SiC, WSi_2, and W_2C, are shown in Figure 14. A more complete description of the refinement results can be found in the Supplementary Material A1. It is possible to observe the presence of peaks not yet indexed as well as some discrepancies between the intensities of the refined peaks and the experimental intensities.

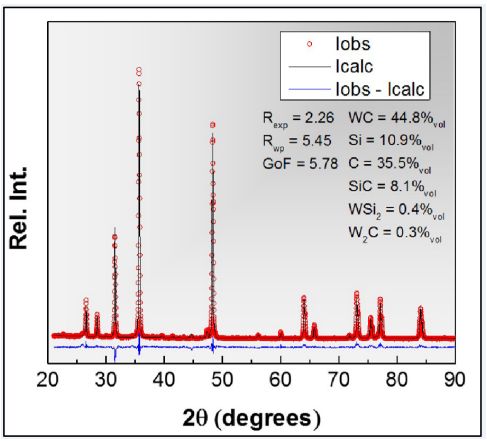

Figure 13. Rietveld refinement of the WC-Co sample after Si and graphite cladding.

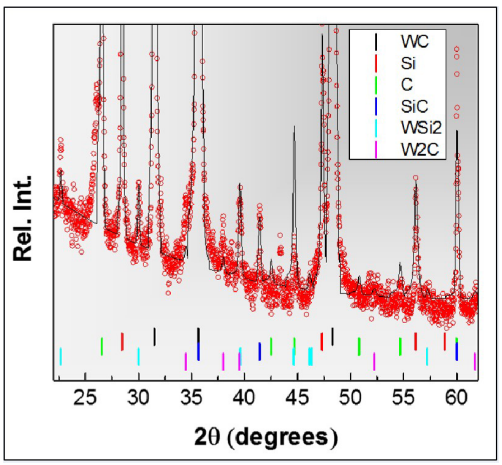

Figure 14. Indexing of the low-intensity peaks present in the XRD of the WC-Co sample after Si and graphite cladding.

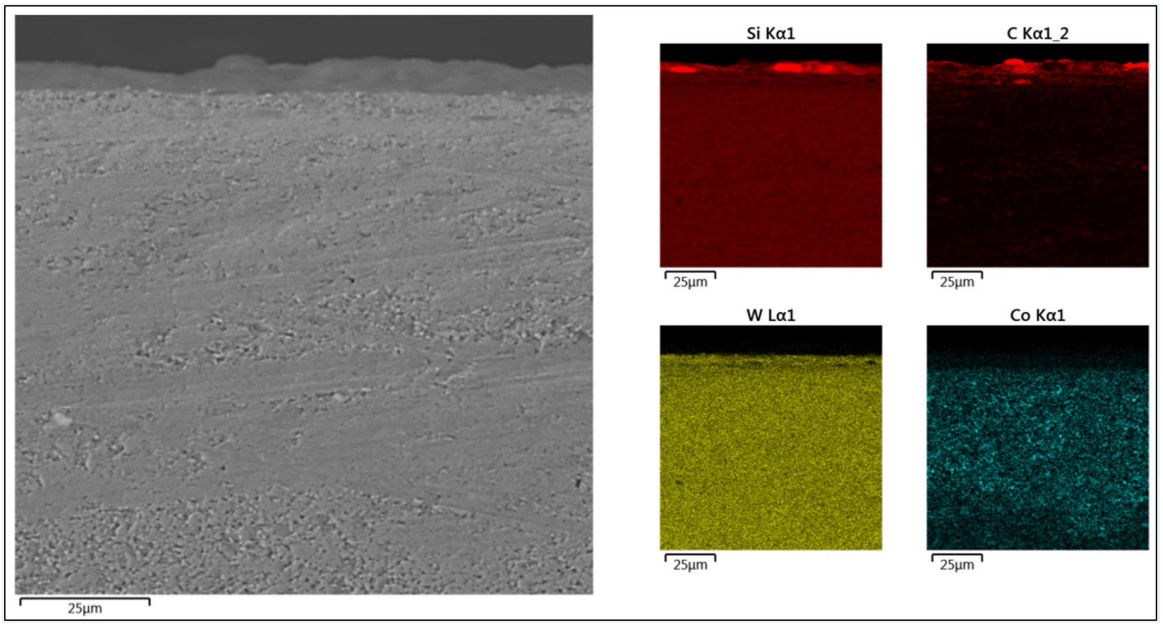

Figure 15. Cross-section of the sample after graphite cladding.

This prevented the achievement of a lower weighted profile R-factor and a good fit suggesting that other phases may be present. Silicon carbide, for example, can have approximately 250 different polytypes. The cubic structure 3C-SiC found in this work is less common than the hexagonal polytype 6H-SiC, but its formation is favored at temperatures above 1400 °C[24], which is consistent with the dissociation of the WC in W_2C and the formation of WSi_2. The presence of the WSi_2 and W_2C phases (Figure 13) is an indication that metallurgical bonding has taken place between the substrate and the coating, as described in Equations 3 and 4, and according to Contin et al.[6], this improves the deposition of the diamond film. However, some fraction of another polytype may be present in a small amount, which makes its identification challenging. Other diffraction techniques, such as grazing incidence angle, would be necessary for a more complete characterization of the present phases.

In the cross-section of the sample after graphite cladding (Figure 15) it is possible to observe a cladded layer of approximately 5µm. Observing the EDS map, shown in Figure 15, it is possible to notice the efficiency of the chemical attack process whose minimizes the presence of cobalt on the sample surface. The results also show a heterogeneous layer with low Si and C concentrations that must be further studied to improve the spraying process or even to reproduce the process for thicker and more homogeneous layers. As the boiling temperature of cobalt is much lower than that of tungsten, a pulsed laser could replace the chemical process to perform cobalt removal and increase the productivity. It should be studied in a future work.

4. Conclusion

A two-step method for the deposition of a SiC layer on the surface of the WC-Co substrate, using silicon and graphite elemental powder, was developed. From the analysis performed in this work, it is possible to conclude the following:

- A low laser energy of 0.27 J was enough to fuse the silicon pre-deposited coating and no chemical reaction was observed between silicon and the WC substrate;
- An even lower laser energy of 0.13 J promoted the reaction of the pre-deposited graphite with the silicon layer and the WC, forming SiC and WSi_2, and this is due to the higher graphite absorptivity at the CO_2 laser wavelength;
- The presence of the WSi_2 phase is an indicator that a metallurgical bond takes place between the SiC layer and the WC-Co substrate;
- Coating adherence was higher in the chemically treated sample due to the increased surface roughness;

The versatility and inexpensiveness of the developed method grants itself a potential for application in both laboratory and industrial environments.

5. Acknowledgments

This work was carried out with the support of the Coordenação de Aperfeiçoamento de Pessoal de Nível Superior- Brazil (CAPES) - Financing Code 001. The authors are grateful to the National Institute of Space Research (INPE), specifically the lab LAS for their support.

6. References

1. Torres CS, Schaeffer L. Sinterização do compósito metal duro WC-Co. Rev Eletrônica Mater Process. 2009;43:59-63.
2. Bobzin K. High-performance coatings for cutting tools. CIRO J Manuf Sci Technol. 2017;18:1-9. http://dx.doi.org/10.1016/j.cirpj.2016.11.004.

3. Zhang D, Shen B, Sun F. Study on tribological behavior and cutting performance of CVD diamond and DLC films on Co-cemented tungsten carbide substrates. Appl Surf Sci. 2010;256:2479-89. http://dx.doi.org/10.1016/j.apsusc.2009.10.092.
4. Campos RA, Contin A, Trava-Airoldi VJ, Barquete DM, Corat EJ. CVD of alternated MCD and NCD films on cemented carbide inserts. J ASTM Int. 2011;8(3):369-82.
5. Wang H, Webb T, Bitler JW. Study of thermal expansion and thermal conductivity of cemented WC-Co composite. Int J Refract Met Hard Mater. 2015;49:170-7. http://dx.doi.org/10.1016/j.ijrmhm.2014.06.009.
6. Contin A, Vasconcelos G, Barquete DMI, Campos RA, Trava-Airoldi VJ, Corat EJ. Laser cladding of SiC multilayers for diamond deposition on steel substrates. Diam Relat Mater. 2016;65:105-14. http://dx.doi.org/10.1016/j.diamond.2016.02.007.
7. Hei H, Shen Y, Ma J, Li X, Yu S, Tang B, et al. Effect of substrate temperature on SiC interlayers for diamond coatings deposition on WC-Co substrates. Vacuum. 2014;109:15-20. http://dx.doi.org/10.1016/j.vacuum.2014.06.001.
8. Silva JV No, Rodríguez LAA, Fraga MA, Contin A, Campos RA, Corat EJ, et al. WC-Co substrate preparation and deposition conditions for high adhesion of CVD diamond coating. Rev Bras Apl Vácuo. 2016;35:53. http://dx.doi.org/10.17563/rbav.v35i1.1015.
9. Barletta M, Rubino G, Gisario A. Adhesion and wear resistance of CVD diamond coatings on laser treated WC-Co substrates. Wear. 2011;271:2016-24. http://dx.doi.org/10.1016/j.wear.2011.01.042.
10. Liu ZL, Xiang L. Effects of working pressure and substrate temperature on the structure and mechanical properties of nanocrystalline SiC thin films deposited by bias-enhanced hot filament chemical vapor deposition. Thin Solid Films. 2014;562:24-31. http://dx.doi.org/10.1016/j.tsf.2014.03.024.
11. Yuan Z, Guo Y, Li C, Liu L, Yang B, Song H, et al. New multilayered diamond/β-SiC composite architectures for high-performance hard coating. Mater Des. 2020;186:108207. http://dx.doi.org/10.1016/j.matdes.2019.108207.
12. Hei H, Yu S, Shen Y, Li X, Ma J, Tang B, et al. Growth of β-SiC interlayers on WC-Co substrates with varying hydrogen/tetramethylsilane flow ratio for adhesion enhancement of diamond coatings. Surf Coat Tech. 2015;272:278-84. http://dx.doi.org/10.1016/j.surfcoat.2015.03.054.
13. Wang T, Zhuang H, Jiang X. One step deposition of highly adhesive diamond films on cemented carbide substrates via diamond/β-SiC composite interlayers. Appl Surf Sci. 2015;359:790-6. http://dx.doi.org/10.1016/j.apsusc.2015.10.165.
14. Cabral G, Gäbler J, Lindner J, Grácio J, Polini R. A study of diamond film deposition on WC-Co inserts for graphite machining: effectiveness of SiC interlayers prepared by HFCVD. Diam Relat Mater. 2008;17:1008-14. http://dx.doi.org/10.1016/j.diamond.2008.03.017.
15. Cui YX, Shen B, Sun FH. Diamond deposition on WC-Co substrate with amorphous SiC interlayer. Surf Eng. 2014;30:237-43. http://dx.doi.org/10.1179/1743294414Y.0000000250.
16. Costa AK, Camargo SS Jr. Properties of amorphous SiC coatings deposited on WC-Co substrates. Mater Res. 2003;6:39-42. http://dx.doi.org/10.1590/s1516-14392003000100007.
17. Wang T, Xiang L, Shi W, Jiang X. Deposition of diamond/β-SiC/cobalt silicide composite interlayers to improve adhesion of diamond coating on WC-Co substrates by DC-Plasma Assisted HFCVD. Surf Coat Tech. 2011;205:3027-34. http://dx.doi.org/10.1016/j.surfcoat.2010.11.014.
18. Sun K, Wang T, Gong W, Lu W, He X, Eddings EG, et al. Synthesis and potential applications of silicon carbide nanomaterials / nanocomposites. Ceram Int. 2022;48(22):32571-87. https://doi.org/10.1016/j.ceramint.2022.07.204
19. Taylor A, Klimsa L, Kopecek J, Remes Z, Vronka M, Ctvrtlík R, et al. Synthesis and properties of diamond - silicon carbide composite layers. J Alloys Compd. 2019;800:327-33.
20. Fang S, Klein S, Bähre D, Llanes L. Performance of laser surface textured cemented carbide tools during abrasive machining: coating effects, surface integrity assessment and wear characterization. CIRO J Manuf Sci Technol. 2020;31:130-9.
21. Ma NN, Chen J, Huang ZR, Li YJ, Liu M, Zhu M, et al. Joining of sintered SiC ceramics at a lower temperature using borosilicate glass with laser cladding Si modification layer. J Eur Ceram Soc. 2021;41(4):2974-8.
22. Yoshida K, See C-C, Yokoyama S, Yano T. (2015). Effects of sic particle size and sintering temperature on microstructure of porous SiC ceramics based on in-situ grain growth. In 38th International Conference on Advanced Ceramics and Composites (Vol. 35, pp. 173-183). Hoboken: John Wiley & Sons. https://doi.org/10.1002/9781119040392.ch15
23. Jana DC, Barick P, Saha BP. Effect of sintering temperature on density and mechanical properties of solid-state sintered silicon carbide ceramics and evaluation of failure origin. J Mater Eng Perform. 2018;27:2960-6. http://dx.doi.org/10.1007/s11665-018-3397-4.
24. Tóth S, Németh P, Rácz P, Himics L, Dombi P, Koós M. Silicon carbide nanocrystals produced by femtosecond laser pulses. Diam Relat Mater. 2018;81:96-102. http://dx.doi.org/10.1016/j.diamond.2017.11.014.
25. Galvão N, Vasconcelos G, Pessoa R, Machado J, Guerino M, Fraga M, et al. A novel method of synthesizing graphene for electronic device applications. Materials (Basel). 2018;11:1-11. http://dx.doi.org/10.3390/ma11071120.
26. Teleginski V, Vasconcelos G. Deposição de revestimentos com laser de CO2 para proteção térmica de palhetas de turbinas aeronáuticas e industriais [thesis]. São José dos Campos: ITA; 2016 [cited 2022 Apr 13]. Available from: http://search.ebscohost.com/login.aspx?direct=true&AuthType=ip,uid&db=cat00958a&AN=ita.72723&lang=pt-br&site=eds http://www.bdita.bibl.ita.br/tesesdigitais/lista_resumo.php?num_tese=72723
27. Chagas DC, Vasconcelos G. Deposição de NiCrAlY em inconel 718 via laser de CO2 [dissertation]. São José dos Campos: ITA; 2016. [cited 2022 Apr 13]. Available from: http://www.bdita.bibl.ita.br/tesesdigitais/lista_resumo.php?num_tese=71857
28. Steen WM, Mazumder J. Laser material processing. 4th ed. London: Springer; 2010. https://doi.org/10.1007/978-1-84996-062-5.
29. Gedda H. Laser cladding: an experimental and theoretical investigation [thesis]. Luleå: Luleå University of Technology; 2004.
30. Thakur D, Ramamoorthy B, Vijayaraghavan L. Influence of different post treatments on tungsten carbide-cobalt inserts. Mater Lett. 2008. http://dx.doi.org/10.1016/j.matlet.2008.07.043.
31. Nanda Kumar AK, Watabe M, Kurokawa K. Reaction-assisted sintering and platelet growth by adiabatic heating in WC-Si cermets. Scr Mater. 2014;75:6-9. http://dx.doi.org/10.1016/j.scriptamat.2013.09.024.
32. Guilemany JM, De Paco JM, Nutting J, Miguel JR. Characterization of the W2C phase formed during the high velocity oxygen fuel spraying of a WC + 12 pct Co powder. Metall Mater Trans, A Phys Metall Mater Sci. 1999. http://dx.doi.org/10.1007/s11661-999-0002-3.
33. Chandler-Horowitz D, Amirtharaj PM. High-accuracy, midinfrared (450 cm -1 ≤ω≤4000 cm -1) refractive index values of silicon. J Appl Phys. 2005;97. http://dx.doi.org/10.1063/1.1923612.
34. Hagemann HJ, Gudat W, Kunz C. Optical constants from the far infrared to the x-ray region: Mg, Al, Cu, Ag, Au, Bi, C, and Al2O3. J Opt Soc Am. 1975. http://dx.doi.org/10.1364/JOSA.65.000742.

Supplementary Material

The following online material is available for this article:

Supplementary Material A1